Hindawi
Science and Technology of Nuclear Installations
Volume 2019, Article ID 6021346, 19 pages
https://doi.org/10.1155/2019/6021346

Research Article

Standalone Containment Analysis of Four Phébus Tests with the ASTEC and the MELCOR Codes

Bruno Gonfiotti and Sandro Paci

University of Pisa, Dipartimento di Ingegneria Civile e Industriale (DICI), Largo Lucio Lazzarino 2, 56122, Pisa, Italy

Correspondence should be addressed to Bruno Gonfiotti; bruno.gonfiotti@for.unipi.it

Received 4 July 2018; Accepted 8 November 2018; Published 1 January 2019

Academic Editor: Alejandro Clausse

After the severe accident (SA) occurred at the Three-Miles Island Nuclear Power Plant (NPP), important efforts on the investigation of the different phenomena during this kind of accidents have been started. Several experimental campaigns investigating one phenomenon at time or the combination of two or more phenomena have been performed. Today, the Phébus experimental campaign is probably the most important activity on the evaluation of the coupling among different phenomena. Four out of five tests investigated the degradation of an intact Pressurized Water Reactor (PWR) fuel bundle and the subsequent transport of Fission Products (FP) and Structural Materials (SM) through the primary circuit and into the containment, while the fifth test was only the degradation of a bed of PWR fuel bundle debris. These tests were performed between 1990 and 2010 at the CEA Cadarache laboratories (France) in a 5000:1 scaled facility. The main four tests varied the employed control rod materials, the fuel burn-up, and the oxidizing conditions of the atmosphere (strongly or weakly). The outcomes of this experimental campaign created a solid base for the understanding of the involved phenomena and allowed the development of models and software codes capable of simulating the evolution of a SA in a real NPP. ASTEC and MELCOR were two of the main SA codes profiting from the results of this Phébus campaign. These two codes were further improved in the latest years to account for the findings obtained in more recent experimental campaigns. A continuous verification and validation work is then necessary to check how the newer code's versions reproduce the tests performed in these older experimental campaigns such as Phébus one. The present work is intended to be the final step of a series of publications covering the activities carried out at University of Pisa with the ASTEC and the MELCOR SA codes on the four Phébus tests employing an intact PWR fuel bundle. Because of the complexity and the extent of these tests, only the containment aspects were considered in the precedent works, i.e., only the thermal-hydraulics transient and its coupling with the FP and SM behavior. Then, general conclusions based on the outcomes of these precedent works are summarized in this work.

1. Introduction

After the Three-Miles Island Severe Accident (SA), important national and international projects and experimental campaigns have been carried out to get a better understanding of the key phenomena occurring in these kinds of accidents [1]. Among all these efforts, only the international Phébus FP experimental programme was devoted to the reproduction of a SA from the initiating event up to the release of radioactive substances into a Containment Vessel (CV) [2]. This experimental campaign was conducted between 1998 and 2010 in the integral Phébus FP facility at the CEA Cadarache laboratories (France) in a 5000:1 scaled facility. The experimental campaign consisted of five integral tests differing in the fuel burn-ups, control rod materials, and thermal-hydraulic conditions investigated [3]. These tests investigated the key processes occurring in a SA: the degradation of the fuel rods, the release of Fission Products (FP) and Structural Materials (SM), and their subsequent transport through the primary circuit and into the containment [4–6]. The Phébus research program provided a comprehensive improvement of the understanding of the key SA phenomena. Furthermore, because of the complexity of these tests and the quality of the results obtained, these tests formed a valuable validation database for several SA codes [1].

Previous analyses (both full-plant and standalone containment) employed too complex [7] or too coarse [8–12] nodalisations. For this reason, three different nodalisations

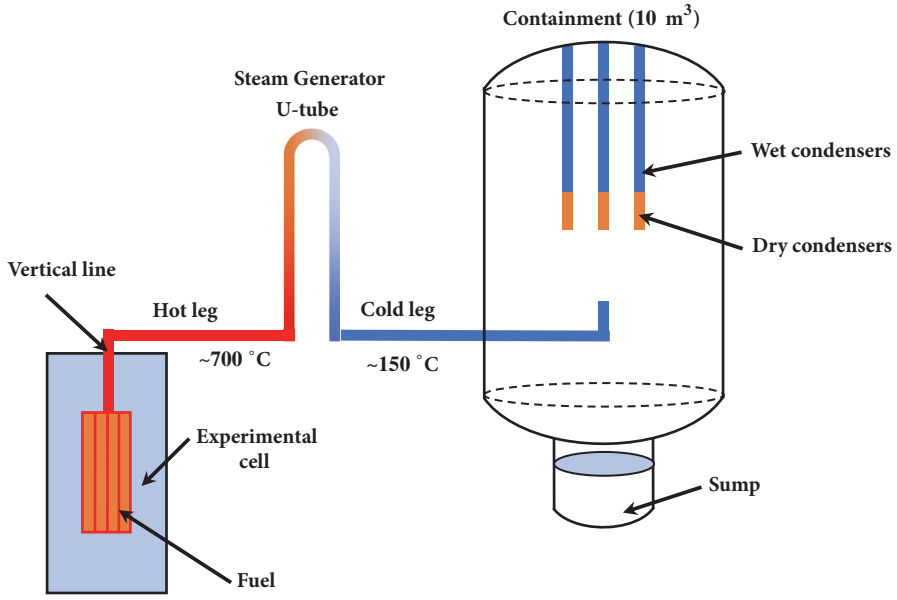

Figure 1: Schematic view of the Phébus FP facility.

were developed to investigate the influence of the CV spatial subdivision. These nodalisations were described in the most identical way possible for both codes, but the different modelling approaches of certain aspects were all exploited to show the capabilities of each code. Quite extended sensitivity analyses were also carried out to investigate the influence of the different code's parameters on the thermal-hydraulic, the aerosol, and FP results.

Then, the present paper summarizes the activities performed on the analysis of the containment aspects of the Phébus FPT-0, 1, 2, and 3 tests. The aim of all these activities was to investigate the main parameters influencing the FP and SM behavior in the CV during the four main phases of each test (degradation, aerosol, washing, and chemistry phases). These analyses were performed with recent ASTEC and MELCOR code's versions to evaluate the effects of the improvements and modifications implemented in both of them in the latest years to account for the new findings from international researches [13, 14]. The present paper is the last of five publications covering the Phébus tests executed with a solid PWR fuel bundle (FPT-0 [15], FPT-1 [16], FPT-2 [17], and FPT-3 [18] tests).

2. The Phébus FP Facility

The Phébus facility is a 5000:1 reproduction of typical French 900 MWe-class Pressurized Water Reactor (PWR) [19–22]. A schematic view of the facility is shown in Figure 1 [2]. The first component is the driver core and its cooling circuit, encapsulated inside a cylindrical shroud. The core consists of a PWR fuel bundle, two instrumented fuel rods, and a control rod. Different fuel burn-up levels and control rod materials were investigated in each Phébus test (Table 1).

During these tests, the driver core is heated up and irradiated to recreate the temperature increase occurring during a Loss Of Coolant Accident (LOCA) and the FP build-up during normal operations. A steam injection occurs at the bottom of the fuel bundle to reproduce different oxidizing atmospheres (dry atmosphere or wet atmosphere). A vertical line at the top of the shroud guides steam, noncondensable gases, FP, and SM into the downscaled primary circuit. The primary circuit consists of three parts:

(i) the first part, made of Inconel-600, simulates the hot leg (700°C);

(ii) the second part, made of Inconel-600, simulates the U-tube type SG;

(iii) the third and last part, made of AISI 304L stainless steel, simulates the cold leg (150°C), ending in the CV.

This CV is a cylindrical shaped volume (10 m^3 free volume, 1.8 m inner diameter, and 5 m in height) with a sump on the lower part. The sump dimensions (0.584 inner diameter and 0.6 m in height) are set to reproduce a representative atmosphere-water exchange surface [11]. Semiellipsoidal structures close the CV top, connect the main cylindrical zone with the sump zone, and close the bottom of the sump. The CV outer walls (made of AISI 316L stainless steel) are temperature-controlled through two independent systems: one for the main cylindrical zone and another for the sump zone. The aim of these independent systems is to decouple the atmospheric temperature from the sump water one. A spray system is also installed in the lower containment zone to wash down the FP and SM settled on the bottom vessel surfaces. The spray covers the entire flow-through area of the cylindrical part, and it is fed only by the water contained in the sump.

Three condensers are attached at the top of the vault to simulate the cold structures of a reactor building. The main aim of these condensers is to allow the control of the heat transfer and steam condensation. Each condenser has an external diameter of 0.15 m and a height of 2.5 m, and it is subdivided into two parts: the "dry" part of 0.782 m and

Table 1: Main characteristics of the different Phébus tests with a solid fuel bundle.

Test	Fuel	Fuel Degradation	Primary Circuit	Containment
FPT-0	Fresh Fuel 1 Ag–In–Cd rod 9 days pre-irradiation	Melt Progression and FP release in steam-rich environment	FP chemistry and deposits in non-condensing steam generator	Aerosol deposition and iodine radiochemistry at pH5
FPT-1	BR3 fuel ≈ 23 GWd/tU 1 Ag–In–Cd rod Re-irradiation	As FPT-0 with irradiated fuel	As FPT-0	As FPT-0
FPT-2	As FPT-1	As FPT-1 under steam poor conditions	As FPT-1 with effect of boric acid	pH9 evaporating sump
FPT-3	As FPT-1 with B_4C instead of Ag–In–Cd	As FPT-2	As FPT-0	pH5 evaporating sump recombiner coupons

the "wet" part of 1.718 m. Total surface area of condensers is about 3.5 m^2: 2.4 m^2 the wet part and 1.1 m^2 the dry part. To ensure condensation only on the condenser wet part, each condenser has two independent cooling systems. The wet part is also covered with an epoxy paint, to allow the formation of organic iodine.

3. The Phébus FPT Tests

The Phébus FPT tests consist of four different phases:

(i) The degradation phase in which the driver core is heated up to allow the progressive melting of the fuel bundle and the subsequent release of FP and SM: during this phase, a continuous steam injection is performed at the bottom of the driver core. The magnitude of these steam injections creates the different atmospheric conditions near the fuel rod bundle (highly or weakly oxidizing conditions) characterizing each test. In this phase, a strong H_2 production also occurs due to the progressive reaction between the steam and the zircaloy clads encapsulating the UO_2 fuel pellets. The injected steam, the produced H_2, the FP, and SM are then transported through the primary circuit into the CV. FP and SM settle onto the containment surfaces, H_2 accumulates on the top of the free CV volume, and steam condenses on the wet condensers surface. The two main aspects that characterize this phase are the fuel burn-up and the steam amount near the fuel bundle. A summary of the fuel burn-up is reported in Table 1, while the amount of steam flowing into the CV during the four different tests is reported in Figure 2.

(ii) The aerosol phase, with the CV maintained in stable conditions and isolated from the driver core: the CV is initially at atmospheric pressure and filled with a mixture of N_2 (~ 95%) and O_2 (~5%) to avoid hydrogen deflagration/detonation. The isolation of the CV occurs through a valve placed in the cold leg prior its ingress into the vessel. From now on the primary circuit and the CV start to evolve independently. The stable conditions in which it is kept allow the settling of the FP and SM aerosol onto the stainless-steel surfaces and into the sump water. Steam condensation onto the wet condensers is also prevented in this phase.

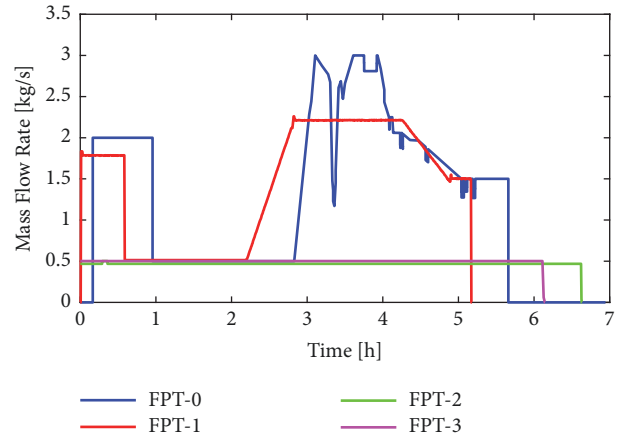

Figure 2: Steam flowing into the CV during the Phébus FPT tests.

(iii) The washing phase in which the FP and the SM that settled onto the CV elliptic bottom are washed down thanks to the activation of the spray: this phase is mainly devoted to the collection of FP and SM into the sump water to allow the investigation of the iodine behavior in the following chemistry phase. In this phase, the CV is still kept isolated from the primary circuit, and the temperature of both parts of the condensers is decreased to allow the condensation of

Table 2: Phase subdivision and timings of the Phébus FPT tests.

Test	Degradation	Phases			
		Aerosol	Washing	Chemistry	End of test
FPT-0	0 s	20,438 s / 5.67 h	111,218 s / 30.9 h	112,118 s / 31.1 h	433,848 s / 120.5 h
FPT-1	0 s	17,039 s / 4.73 h	250,000 s / 60.4 h	251,260 s / 69.8 h	341,400 s / 94.8 h
FPT-2	0 s	24,240 s / 6.73 h	157,140 s / 43.7 h	177,060 s / 49.2 h	375,780 s / 104.4 h
FPT-3	0 s	22,500 s / 6.25 h	151,920 s / 42.2 h	184,440 s / 51.2 h	386,340 s / 107.3 h

Table 3: Main initial conditions of the Phébus FPT tests.

Test	Total pressure [MPa]	Relative humidity [-]	Atmosphere composition [O_2% / N_2%]	Sump water mass [kg]	Temperature [°C]	
					Water	Atmosphere
FPT-0	0.195	0.49	5.25 / 94.75	100	90.0	106.0
FPT-1	0.209	0.53	5.0 / 95.0	105	89.3	109.2
FPT-2	0.201	0.51	5.0 / 95.0	110	89.75	108.7
FPT-3	0.209	0.58	3.6 /96.4	110	89.38	107.4

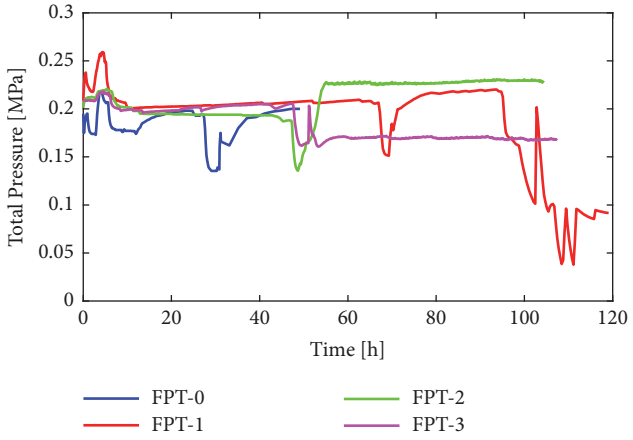

Figure 3: CV total pressure during the Phébus FPT tests.

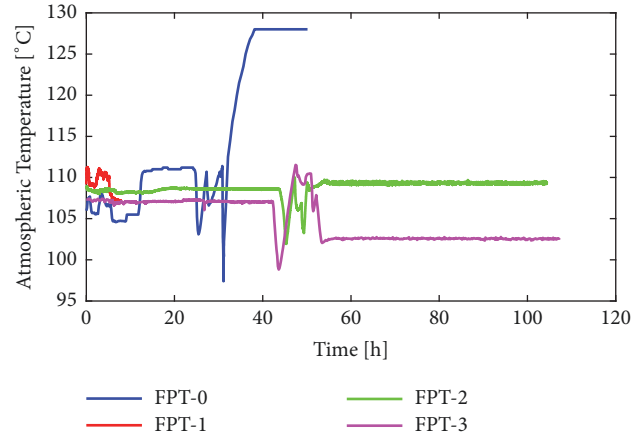

Figure 4: CV mean atmospheric temperature during the Phébus FPT tests.

steam and the subsequent removal of the FP and SM settled on their surfaces.

(iv) The final chemistry phase devoted to the investigation of the iodine behavior in the sump: during this phase, the CV is kept under stable conditions, isolated from the driver core, and the steam condensation onto the condenser surfaces is prevented. Depending on the test, iodine behavior in acid and basic water environments was investigated (Table 1).

The phase subdivision and timings of the different Phébus FPT tests are reported in Table 2, while in Figures 3 and 4 the evolution of the CV thermal-hydraulics conditions in terms of total pressure and mean atmosphere temperature evolution for the different tests are shown (note that in the FPT-1 test Final Report [18] the atmospheric temperature evolution was reported only for the first 8 h of the transient). Finally, the main initial thermal-hydraulics conditions of the different tests are reported in Table 3, while the amount of the different FP and SM entering into the CV is listed in Table 4.

4. Employed Nodalisations

To quantify the influence of spatial nodalisation on the overall results, three CV spatial nodalisations (Figure 5) have been developed. The first model (M1) is quite coarse and it has been mainly created to test the quality of the imposed boundary conditions. The second (M2) and the third (M3) models have been then developed to investigate the influence of the vertical and radial subdivision, respectively.

In all the three models, the sump volume partially enters into the cylindrical zone to avoid too small gaseous phase when the water level increases up to about 0.6 m (small sump gaseous phase might lead to time-step decreases and abnormal calculation terminations [23]). The different volumes are connected by means of flow junctions, and several walls simulate the outer CV surfaces and the

Table 4: Amount of FP and SM flowing into the CV during the Phébus FPT tests.

	Mass [g]			
Element	**FPT-0**	**FPT-1**	**FPT-2**	**FPT-3**
Xe	0.028	22.9	32.37	25.43
Kr	0.263	2.14	2.628	1.924
Te	0.037	1.33	1.057	0.116
I	0.023	0.718	0.883	0.387
Sb	6.4e-4	0.02	\	\
Cs	0.074	6.95	9.182	3.757
Sn	10.1	16.1	3.341	1.618
Cd	5.6	15.2	6.808	\
Co	3.6	\	\	\
Ag	50	32	7.109	0.031
In	7.4	7	5.119	\
W	2	\	0.676	1.012
Re	27	29.4	1.428	0.0724
Mn	4	\	\	\
Ru	2.7e-4	0.056	0.013	0.03
Cr	0.77	\	\	\
Ba	8.9e-4	0.065	0.053	0.068
U	6.9	10.9	0.247	0.065
Sr	2.1e-5	0.017	0.032	0.016
Nb	3.5e-7	\	\	\
Zr	2.4e-5	0.5	0.268	0.05
Sm	\	9.6e-4	\	\
Nd	\	9.e-4	\	\
Np	\	0.013	\	\
Pu	\	0.9	\	\
Al	\	1.9	\	\
Pb	\	1	\	\
Mo	\	4.6	7.235	1.655
Tc	\	1	0.065	0.016
Rb	\	1.2	1.127	0.464
Ce	\	\	0.04	\
Y	\	\	0.003	\
La	\	\	0.006	\
Pm	\	\	0.002	\
B	\	\	\	1.331
Total	**117.8**	**155.9**	**76.7**	**38.0**

wet and dry condensers parts. Walls have been simulated with an imposed temperature evolving in time according to the test's procedures [19–22]. A special attention has been given to the evaluation of the "characteristic length" (often called hydraulic diameter) of each wall: according to the ASTEC/CPA theory manual [23] and from a Sandia National Laboratory report on the nodalisations of PWR containments [24], the correlations reported in (1) have been employed. Though, for the walls simulating the dry and wet condenser's parts, the hydraulic diameter was set equal to their outer diameter because of the better agreement obtained between the calculated and the experimental condensation rates.

Characteristic Length Relations

$$\begin{aligned} &\textit{Vertical cylinders} \longrightarrow CL = \textit{Height of the wall} \\ &\textit{Horizontal surfaces} \longrightarrow \\ &\qquad CL = \frac{\textit{Area of the wall}}{\textit{Perimeter of the wall}} \end{aligned} \tag{1}$$

Additional walls or flow junctions have been also added in both codes for the proper activation of some models:

(i) In both codes, additional walls have been added to the "flow-through" volumes (such as C1, C2, C3, and C4

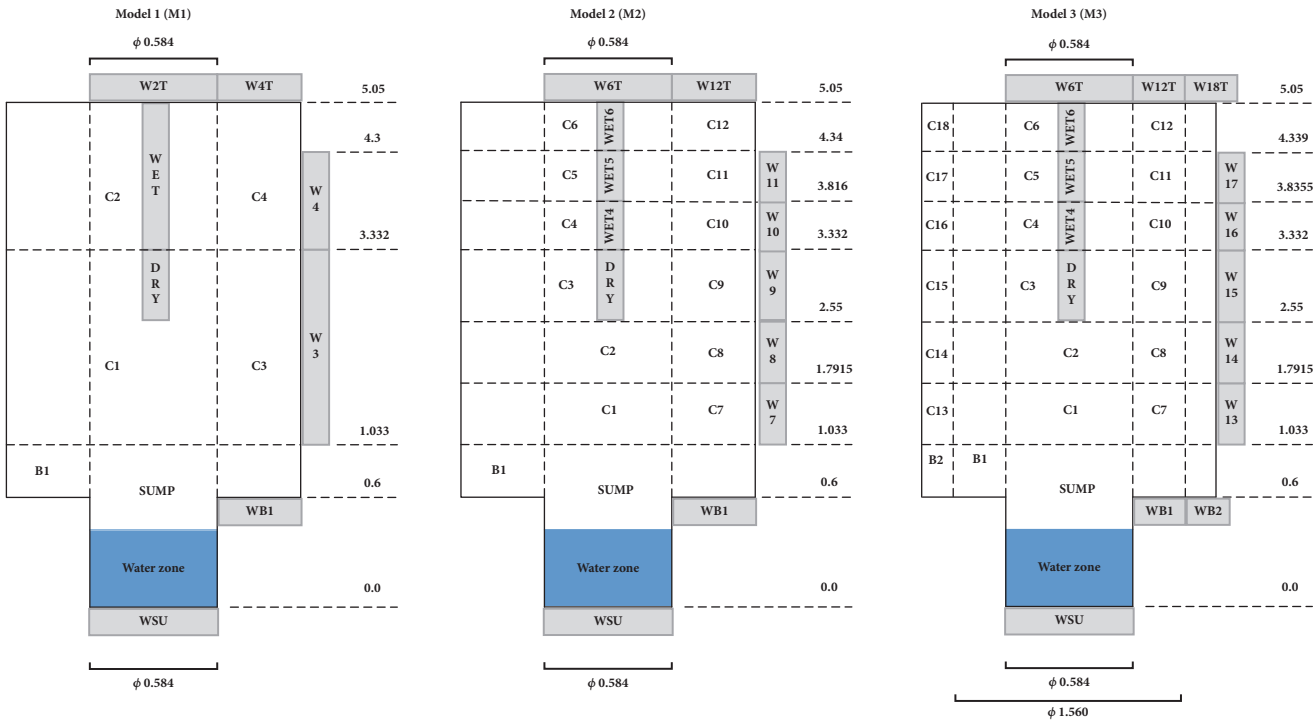

Figure 5: Sketches of the employed CV nodalisations.

of model M1) to provide a settling surface as suggested in the MELCOR User's Manual [25].

(ii) In ASTEC, additional flow junctions have been added to simulate the water draining from the volume containing the wet condenser's part to the sump and the spray injection. ASTEC allows only the discharge of condensed water from a volume to another; thus additional flow paths have been added to reproduce the route from the volume containing the wet condenser's part down to the sump volume. In MELCOR, the same phenomenon can be reproduced with the "film tracking model" which tracks the route of condensed water from a wall placed in an upper position down to walls in lower positions.

(iii) Spray injection is simulated with a specific model in MELCOR, while in ASTEC additional junctions have been employed.

Mass injections and samplings have been placed at the CV centerline at a height of about 1.5 m. Injection and sampling slopes, dose rates, and aerosol characteristics (Aerosol Mass Median Diameter: AMMD and Geometric Standard Deviation: GSD) have been all set according to the data reported in the respective "Final Reports" [19–22].

5. Thermal-Hydraulics Results

For the following analysis of the aerosol behavior is of utmost importance to ensure the proper evaluation of the CV thermal-hydraulics transients. For this reason, a thorough analysis of the thermal-hydraulic transients of each Phébus FPT test has been performed with all the three developed models. As expected, the third model (M3) showed the best agreement between the calculated and the experimental data, but an influence of user's effects and poor boundary conditions was also noted. In the following, only the results of the third model (M3) will be shown and discussed.

For instance, discrepancies start to appear on the total pressure (Figure 6) during the aerosol phase of the FPT-0 and FPT-2 tests. During this aerosol phase condensation on wet condenser's surface, sporadic samplings, and constants noncondensable injections continue to occur. The combination of these three phenomena defines the evolution of the total pressure: if the combination is well predicted the total pressure follows the experimental trend (FPT-1 and FPT-3 tests); otherwise differences appear (FPT-0 and FPT-2 tests). Important differences exist in the quality of the provided experimental data; thus a combined influence of lacking experimental data and user's effect might explain the discrepancies shown.

Similar discrepancies were shown among the different tests at the end of the aerosol phase. In the experiments, the sump water and the superficial wet condenser's temperatures are decreased to prepare the following washing phase while a continuous noncondensable gas injection continues to occur. All these phenomena influence the total pressure which presents an initial decrease due to the enhanced condensation followed by an increase due to the noncondensable gas ingress. Both codes fail to follow this trend probably because of the too strong influence of the condenser and sump water temperatures on the CV atmosphere. The origin of these improper feedbacks probably lies in the employed nodalisations/user's choices being almost identical in both codes and in all the four tests.

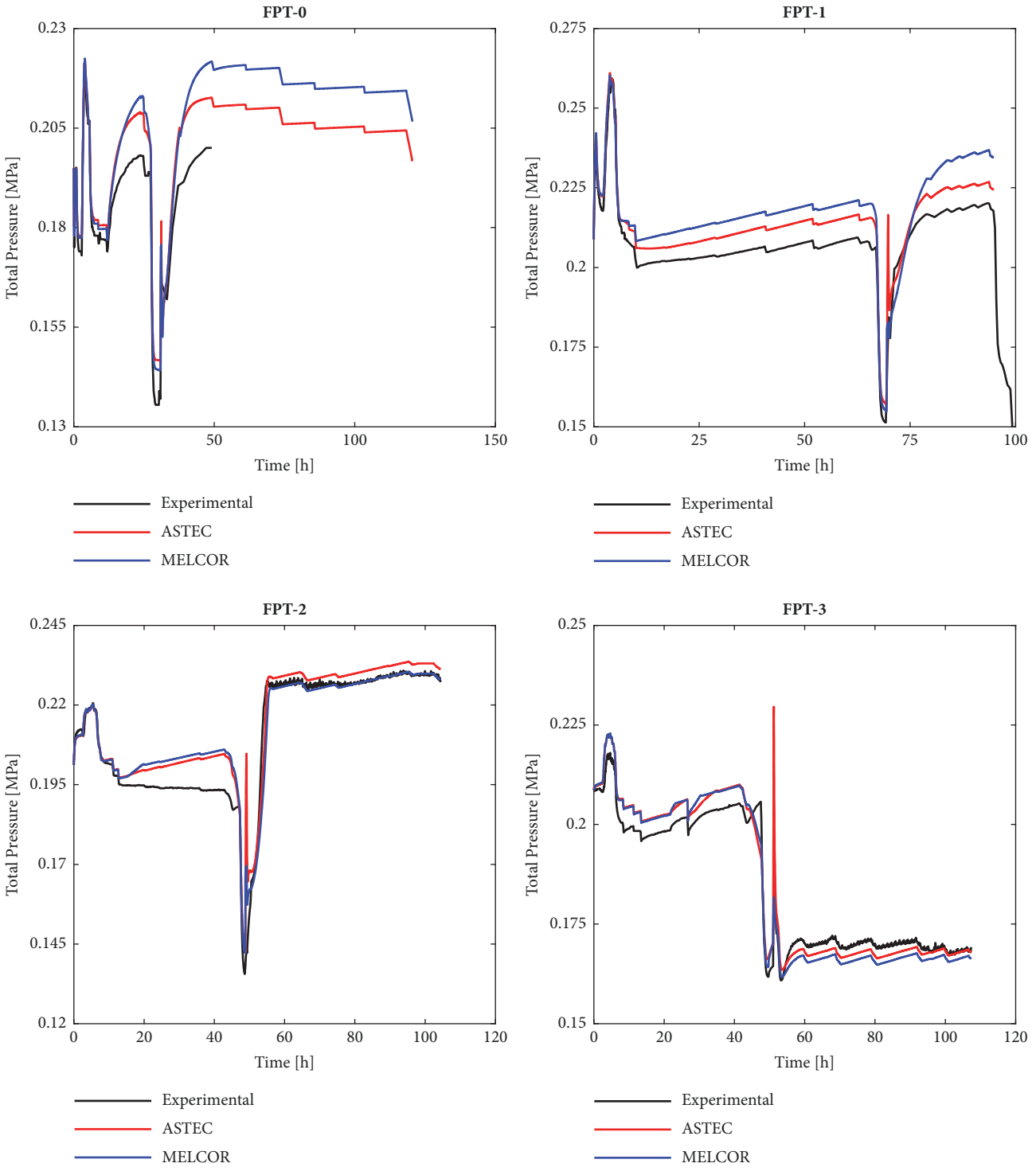

Figure 6: Total pressure evolution during the Phébus FPT tests.

Several discrepancies are also shown during the preparatory phase prior to the washing phase, but this time these differences are also reflected on the mean atmospheric temperature (Figure 7). The different behavior shown among the four tests and between the two codes suggests that the modelling choices of ASTEC and MELCOR play an important role, and a detailed analysis on the nodalisations choices was performed for the FPT-0 and FPT-2 tests. This analysis showed the important influence of the wall's characteristic length values on the condensation rates during the degradation phase and on the atmospheric temperature during the washing phase. For the wet and dry condenser walls, characteristic length values of 0.01–0.02 m were proposed in a precedent work [7], but with the present nodalisation

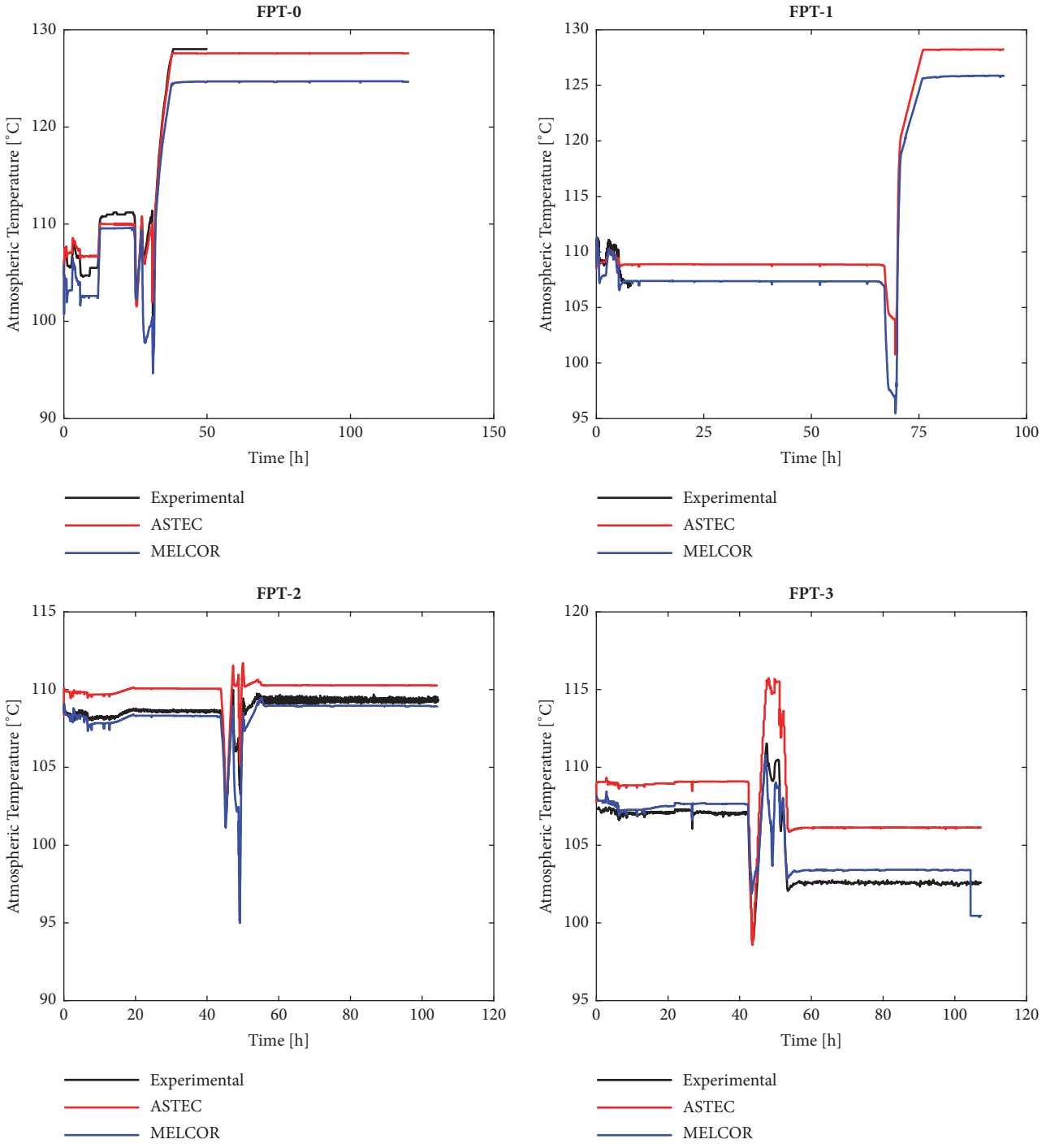

Figure 7: Mean atmospheric temperature evolution during the Phébus FPT tests.

they showed too strong condensation rates. For this reason, a value (0.15 m which is also the outer condensers diameter) capable of reproducing the condensation rate during this initial degradation phase was chosen (Figure 8). The difficulty of reproducing of the experimental condensation rate probably resides in the employed models that are not capable of catching the drop-wise condensation occurring on the condenser's surfaces.

In turn, the characteristic length values of the outer CV walls were investigated with a "try, check, and revise" approach: different values from 0.01 m up to 0.1 m were investigated for the different models in an attempt to define a "scheme" between the nodalisation choices and the characteristic length values reproducing the experimental results more precisely. This last analysis showed that a better reproduction of the FPT-0 and FPT-2 tests can be achieved with

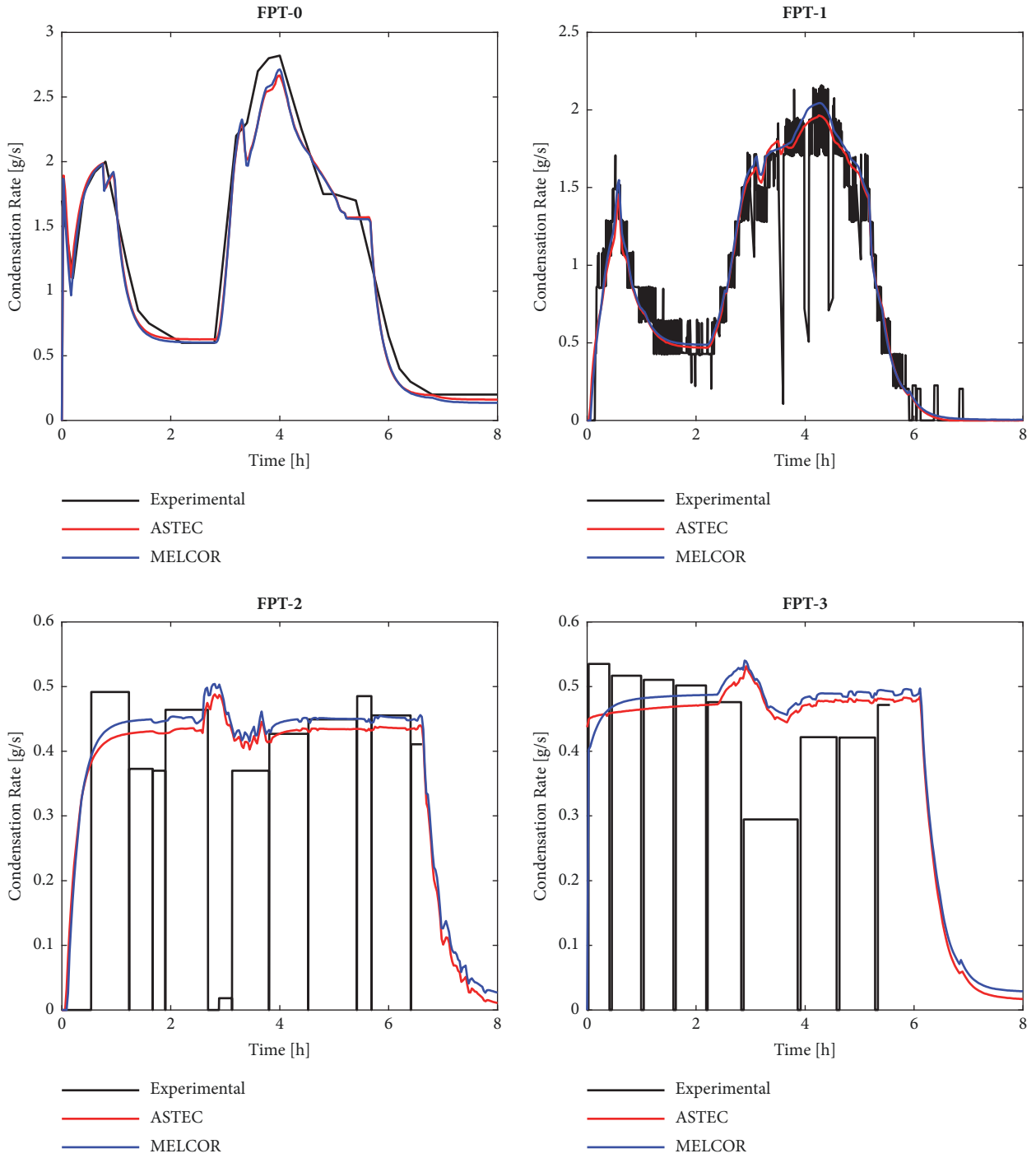

Figure 8: Total condensation rate onto the wet condenser's surface during the degradation phase of the Phébus FPT tests.

some specific characteristic length values, but these values are mainly test-dependent with only a minor influence given by the number of volumes/walls employed in the nodalisation (Table 5). In Figure 9, a comparison between the MELCOR default case and that with modified characteristic length values on the mean atmospheric temperature in the two FPT-0 and FPT-2 tests is shown. The results of this sensitivity analysis suggest that the proper definition of characteristic lengths/hydraulic diameters is still an open question, thus an important source of user's effect on the code's predictions.

Finally, minor uncertainties in the total pressure and relative humidity (r.h.) are also shown during the final chemistry phase in the FPT-0 and FPT-1 tests. In MELCOR, the overestimation of the r.h. (Figure 10) is the cause of discrepancy on the total pressure, while in ASTEC all the other thermal-hydraulic parameters are well captured except the r.h. The FPT-1 test is also affected by an additional user's

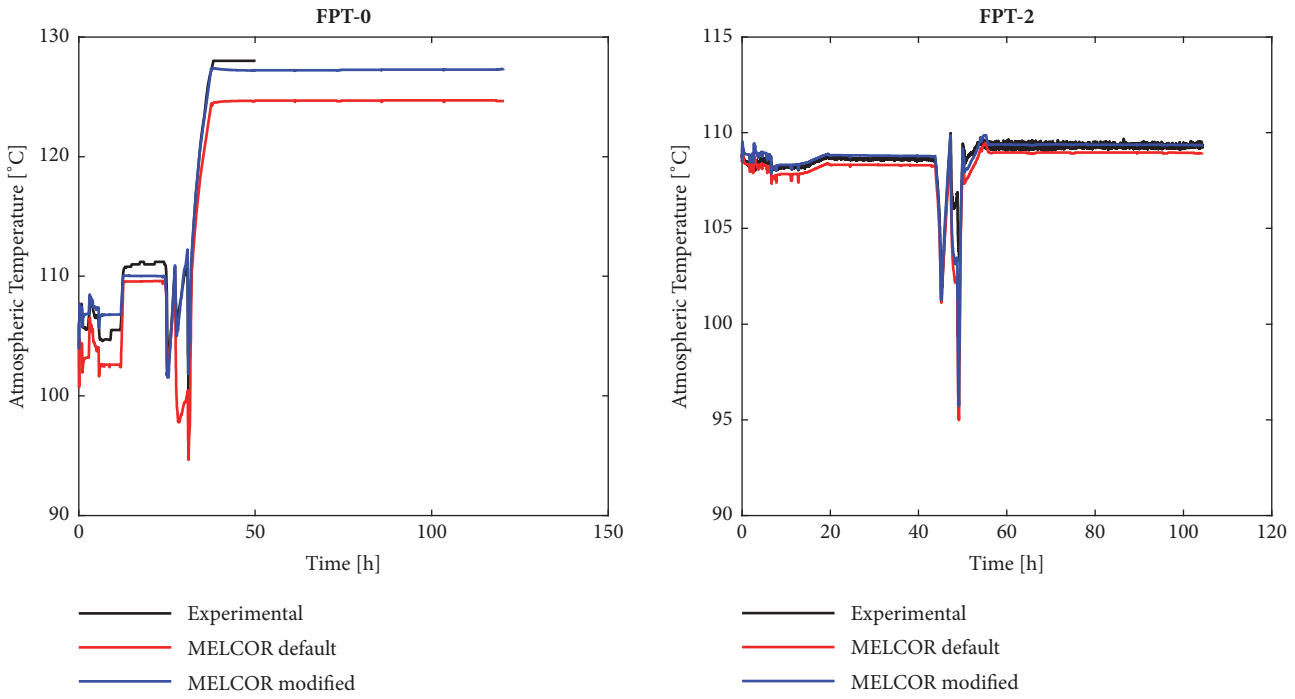

Figure 9: Influence of the outer wall's characteristic length values used by MELCOR on the mean atmospheric temperature during the Phébus FPT-0 and FPT-2 tests.

Table 5: Characteristic length values investigated for the FPT-0 and FPT-2 tests.

	Best-estimation value	
Value [m]	**FPT-0**	**FPT-2**
0.01	M2	
0.015	M1	M2
0.02		M1
0.03		
0.04	M3	
0.05		
0.06		
0.07		M3
0.08		
0.09		
0.1		

effect due to the lack of experimental data: between 69.9 h and 75.8 h no data are provided for the outer vessel wall temperature; hence a linear increase from 120°C up to 130°C was assumed.

Except for the discrepancies pointed out before, the remaining thermal-hydraulic parameters are generally well captured in the different phases of the Phébus FPT tests. The CV atmospheric temperature is always well captured—except during the washing phase and its preparatory phase—with differences not exceeding 3°C in both codes. The maximum r.h. difference does not exceed 10% in all the tests, albeit test-dependent uncertainties are shown for both codes. Finally, the overall condensation rate predictions during the degradation phases of the four Phébus tests agree quite well with the experimental trends, even if localized uncertainties exist for the FPT-2 and FPT-3 tests. These differences are probably due to the difficulties to reproduce the motion of the H_2 plume exiting from the final part of the primary circuit and passing through the CV height. Indeed, the interpretation of the experimental data suggests that the strong ingress of H_2 creates an atmosphere poor in steam in the close vicinity of the condensers thus leading to a drop of the condensation rate. In both codes and tests this phenomenon seems to be not well reproduced: the entering H_2 seems to stop below the condensers pushing upward the atmosphere rich in steam contained in this CV part, thus leading to an increase of the condensation rate instead of a decrease.

6. Fission Product Behaviour

The second part of the analysis on the Phébus FPT tests was focused on the FP and SM behavior. The coupling between the thermal-hydraulic transient and the FP and SM behavior was investigated with all the three developed models, but again the third one was found to provide the closest agreement with the experimental data. The influence of the characteristic length values employed for the outer walls did not affect appreciably the FP and SM behavior.

The analysis of the suspended and deposited FP and SM mass is of utmost importance for the understanding of the capabilities of the two employed codes. The combination of several phenomena guides the evolution of the FP and SM mass: local thermal-hydraulics conditions, different agglomeration processes, and eventual resuspension

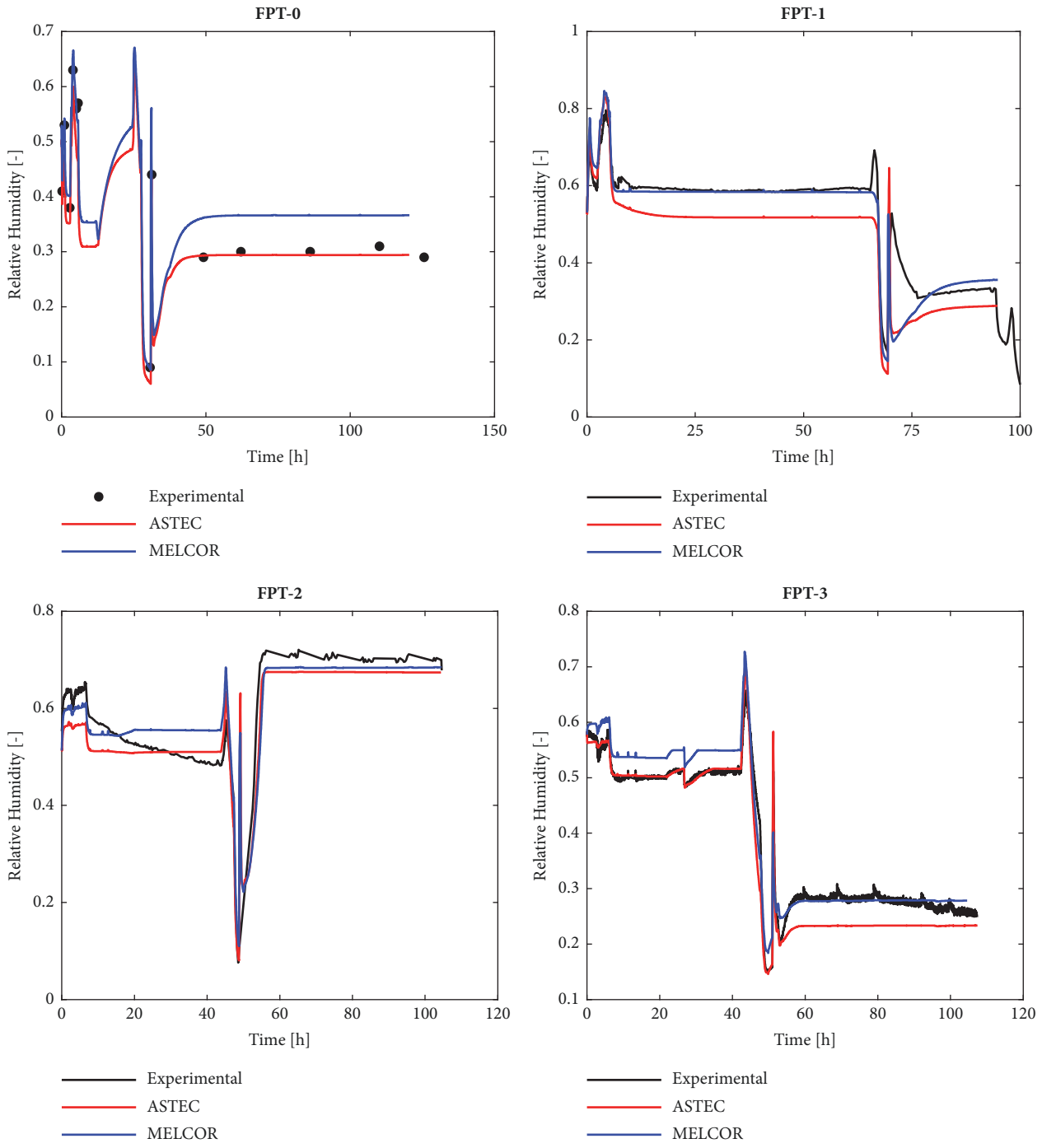

Figure 10: Relative humidity evolution during the Phébus FPT tests.

processes. The combination of all these phenomena is the main difference between the Phébus FPT tests and other simpler tests. According to Figure 11, both codes present a too fast deposition of the FP and SM mass for all the investigated tests. This behavior suggests that a user's effect on the employed nodalisation is present, but this effect plays only a minor role on the overall results since the evolution of the FP and SM mass can be considered acceptable.

Another parameter of interest is the deposition of iodine (and its compounds) on the wet condensers surface. For this parameter, the two codes present very different behavior due to their modelling approaches. Focusing only on the FPT-1 and FPT-2 tests—being the experimental data provided only for these two tests—the ASTEC results are closer to the experimental data than the MELCOR ones (Figure 12). This difference is mainly due to the modelling approach of MELCOR: once condensation occurs on a surface the eventual FP and SM deposited are rapidly washed down by the flowing of the condensate. This behavior can be changed tuning some sensitivity parameters [25], but no modifications

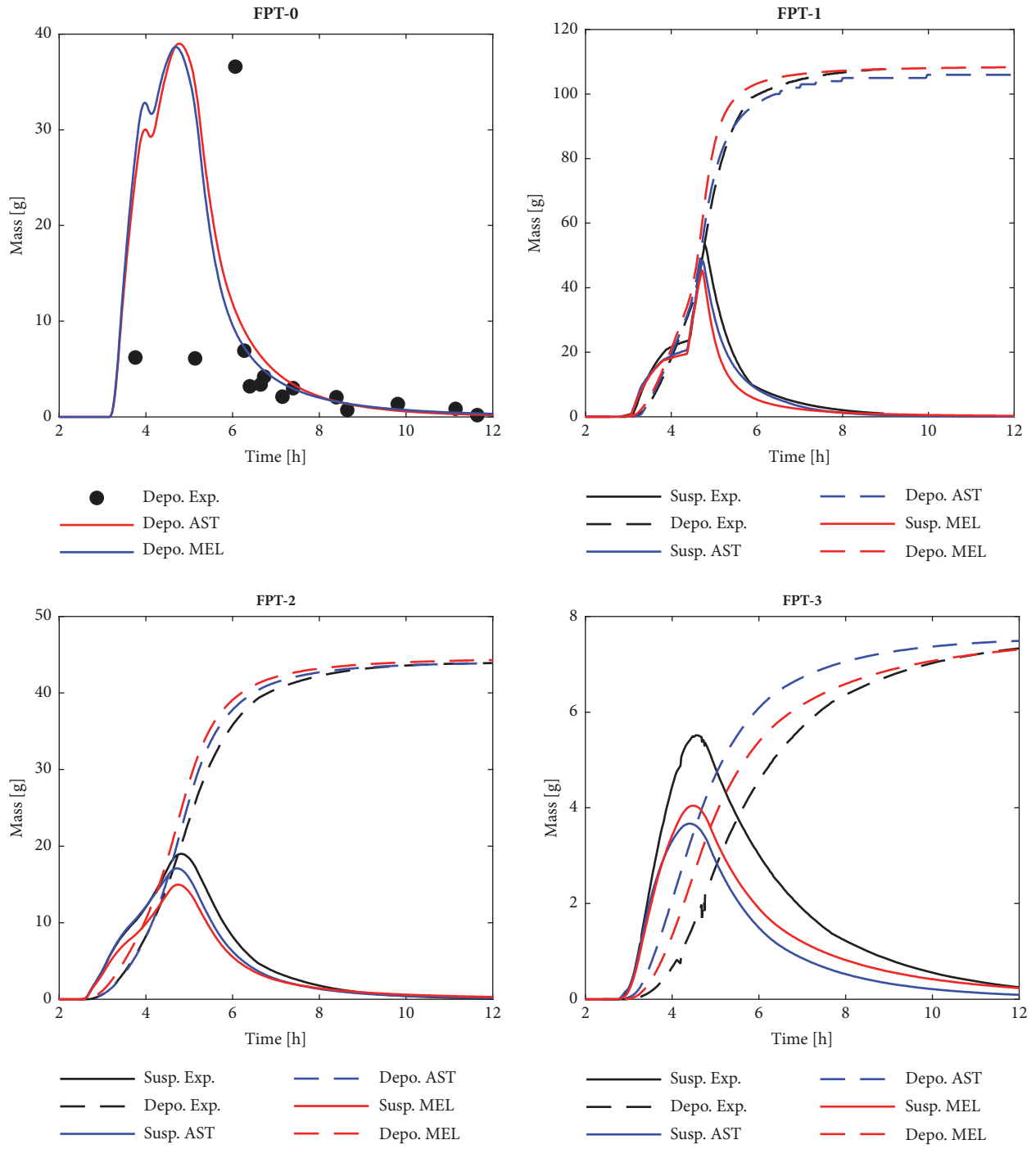

Figure 11: Suspended and deposited aerosol mass during the Phébus FPT tests.

were tried due to the lack of precise data on the dissolution velocity of FP and SM into the condensate film.

Still regarding the iodine behavior, the repartition among the containment atmosphere and the containment surfaces is of interest. A cycle of iodine deposition and resuspension is established between the CV walls and the atmosphere, as well as between the sump water and the atmosphere. The walls-atmosphere cycle is mainly influenced by the dose rates in the atmosphere and on the wall and the sump water-atmosphere cycle by the dose rate in the water and its pH. In the two FPT-1 and FPT-2 tests (Figure 12), two completely different behaviors are shown for both codes: in the FPT-1 test, the concentration of iodine in the atmosphere is quite well predicted, while in the FPT-2 poor results are provided. The cause of this difference is given by the boundary conditions employed: for the FPT-1 test experimental data on the dose evolution are available, while no data exist for the FPT-2 test; thus the dose rates were set as boundary conditions only

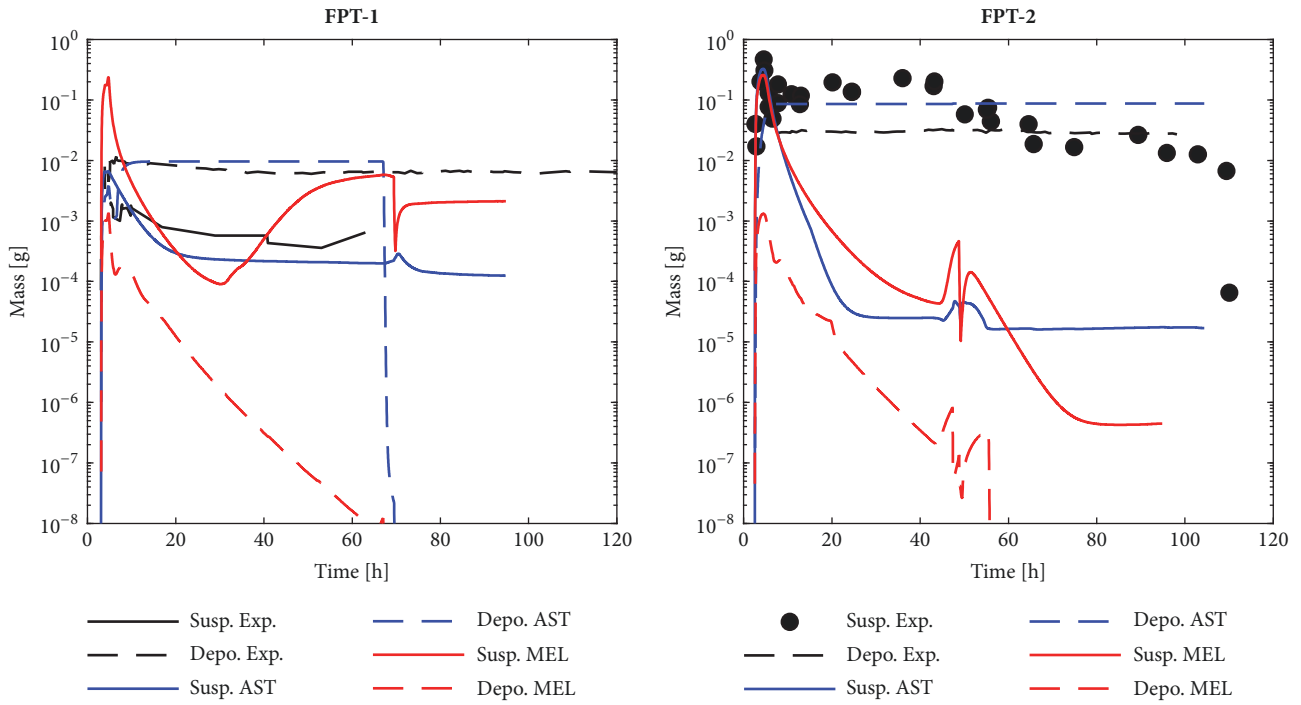

FIGURE 12: Deposited iodine mass on wet condenser's surfaces, and suspended iodine mass in the atmosphere during the Phébus FPT-1 and FPT-2 tests.

for the FPT-1 test. The absence of this boundary condition is probably the most influencing user effect on the FPT-2 calculations: both codes fail to reproduce the creation and destruction cycle of volatile iodine species without the definition of dose rates, thus leading to poor and unrealistic results.

Finally, the speciation of iodine in the sump water is another parameter of utmost importance. In this regard, the two codes provide completely different results because ASTEC implements the most recent findings on iodine chemistry [26], while MELCOR still presents modelling approaches anchored to older researches [27]. The results obtained for each Phébus test are also quite different because of the differences among them: the burn-up of the degraded fuel, the employed control rod materials, and the sump pH. For the FPT-0 test (Figure 13), the two codes present a quite different iodine speciation and mass evolution. Except for the mass difference, the speciation in MELCOR is not so far from the correct one: iodine is mainly found in AgI form, with traces of CsI and I_2 depending on the sump thermal-hydraulics conditions. In ASTEC, the iodine mass is well predicted, and the main formed species is AgI, with traces of I^- at the beginning of the degradation phase and during the washing phase. Less important iodine species are also predicted by both codes depending on the sump thermal-hydraulic conditions. According to [26], iodine should be mainly found in AgI form with traces of I_2 or I^-, but without CsI because of its instability in the CV thermal-hydraulics conditions. Thus, ASTEC presents a very good agreement with the experimental and the theoretical data, while poorer results are shown for MELCOR.

Similarly, the FPT-1 test (Figure 14) presents the same sump conditions of the FPT-0 test (pH of 5), an Ag-In-Cd control rod, but a fuel with a higher burn-up. Though, iodine should be still found as AgI with other forms (I^-, I_2, HIO, etc.) playing only a minor role [26]. Also in this case the two codes present different behaviors: ASTEC again presents a speciation that agrees with [26], while in MELCOR important traces of CsI are still predicted. The two codes also present a very different iodine mass balance (in the sump water), but no experimental data are available for a comparison.

On the contrary, the FPT-2 (Figure 15) has similar conditions of the FPT-0 test, but with a sump in evaporating conditions and a pH of 9. The different state of the sump (evaporating versus condensing) influences the speciation in both codes: in ASTEC important amounts of AgI and I^- are formed, while in MELCOR iodine is still mainly found in AgI form. MELCOR predictions seem still far from that expected from [26] due to important presence of CsI, but the total amount of iodine in the pool before the washing phase is only slightly underestimated. In turn, ASTEC seems to show more reliable results, even if the correct estimation of the repartition between AgI and I^- cannot be ensured due to the lack of specific data.

Finally, the FPT-3 test (Figure 16) is characterized by a sump in evaporating conditions, but with a pH of 5 and a B_4C control rod instead of Ag-In-Cd one as in the previous tests. The presence of a B_4C control rod completely changes the iodine speciation: important amounts of iodine species different than AgI form should be formed throughout the test [26] due to the small availability of Ag, and small amounts of carbonaceous species should appear as well.

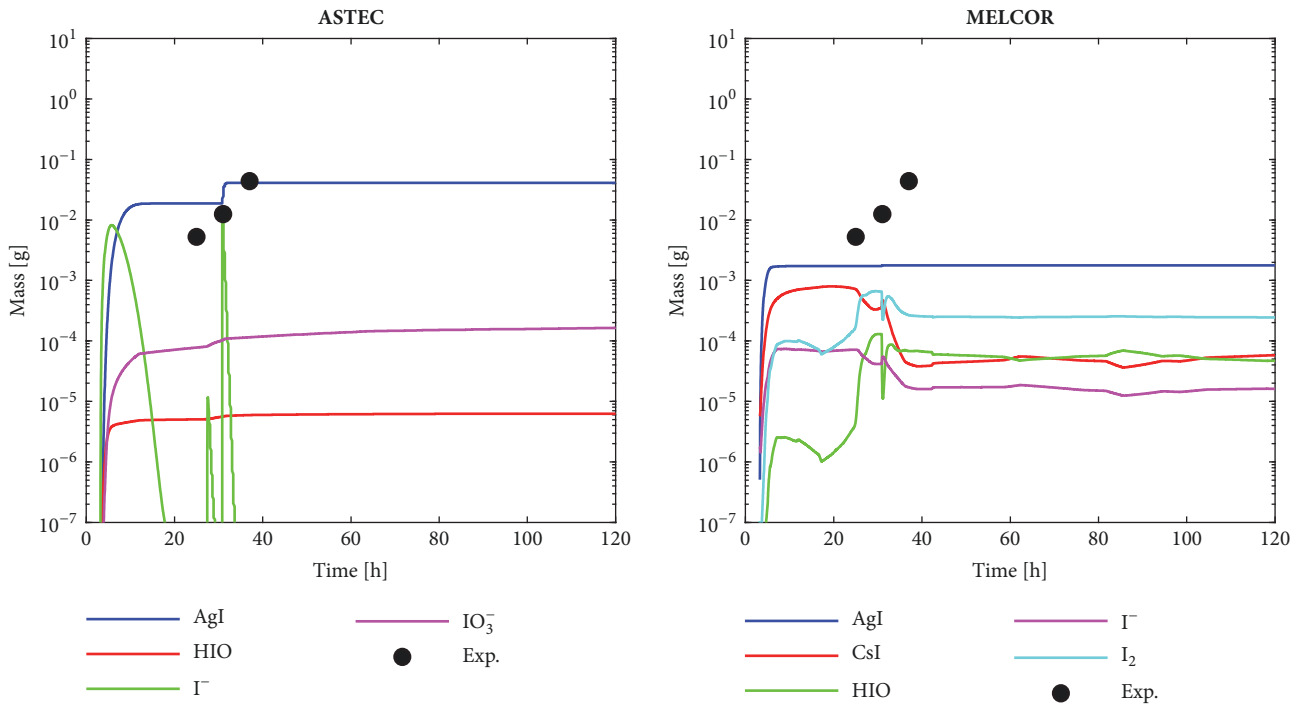

Figure 13: Iodine speciation in the sump water during the Phébus FPT-0 test.

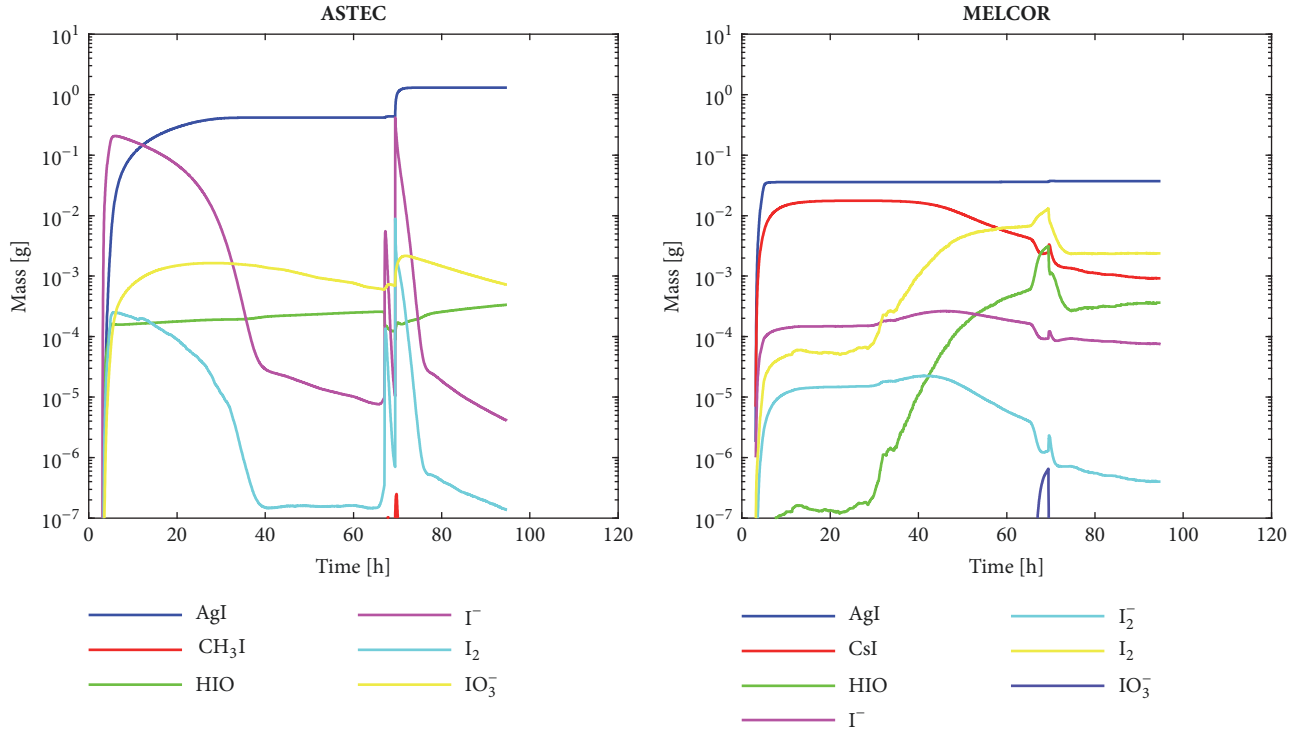

Figure 14: Iodine speciation in the sump water during the Phébus FPT-1 test.

These events are well captured by ASTEC, indeed the main iodine species formed are I^- and AgI (a certain amount of Ag is still present because it is formed during the fuel irradiation process), and small amounts of carbonaceous species are predicted. MELCOR still shows an unrealistic speciation due to the wrong amounts of CsI predicted, and for the complete absence of carbonaceous species. As for the FPT-0 test, the overall iodine mass balance is well captured by ASTEC, while MELCOR fails of about one order of magnitude.

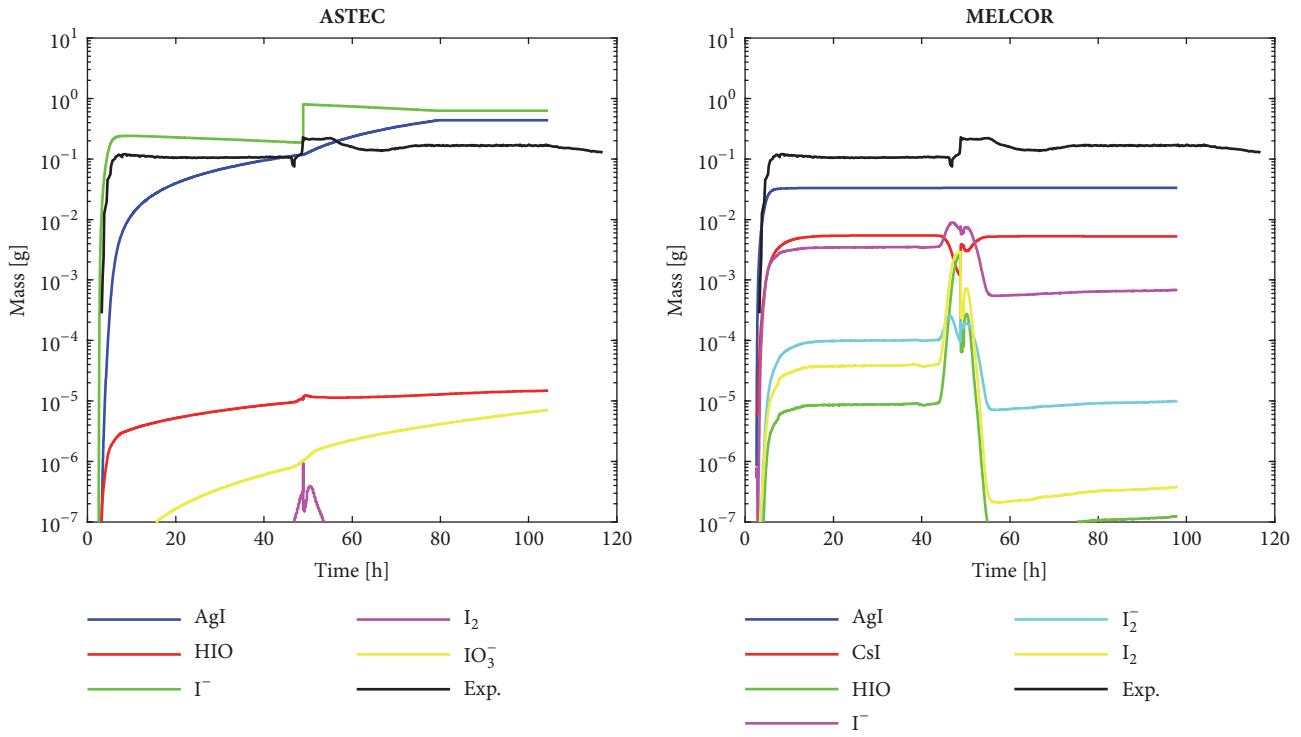

Figure 15: Iodine speciation in the sump water during the Phébus FPT-2 test.

7. Sensitivity Analyses on Aerosol-Related Input Parameters

To get a better understanding of the capabilities of the two codes, a wide set of sensitivity analyses on the aerosol behavior was also performed. The aim of these analyses was to address the overall influence of each input parameter on the obtained results. For this reason, these analyses were performed in a systematic way: same degree of detail for each Phébus test, and—if possible—several values investigated for each parameter.

The first parameter investigated for both codes was the Number of Particle Size Classes (NPSC). This parameter has no physical meaning, but it is the number of intervals (classes) in which the log-normal distribution of the injected aerosols is subdivided. A default value of 10 is suggested for MELCOR, while for ASTEC no default value is provided [25]. Five analyses were performed setting NPSC equal to 10, 20, 30, 40, and 50, and quite different results were highlighted between the FPT-1 test and other ones:

(i) In the FPT-1 test, the results were more scattered: for MELCOR, the cases with NPSC set to 40 and 50 were unable to run due to numerical issues, while for ASTEC these two cases provided quite different results than the other three.

(ii) In the FPT-0, FPT-2, and FPT-3 tests, no appreciable differences were found, except for the increasing calculation time required to run the calculations with high NPSC (>30).

The obtained results show that the NPCS parameter might influence the code results depending on the investigated test, but a value of 20 should be able to catch the experimental trends without a negative impact on the required calculation time.

Four different values (1: default value, 1.5, 2, and 3) for the dynamic shape factor for agglomeration process were also investigated. In both codes, this parameter was found to be of great importance: the increase of the dynamic shape factor seems to reduce the likelihood of agglomeration among particles, thus reducing the deposition velocity because the particles are "lighter". Dynamic shape factors equal to 2 (MELCOR) and 1.5 (ASTEC) showed a better agreement with the experimental and calculated data, but again the influence of this parameter was found to be test-dependent.

Aerosol density was investigated through a set of sensitivity cases: no default density values exist for dry aerosols so a value of 3,000 kg/m^3 was employed, and then values spanning from 1,000 up to 20,000 kg/m^3 were investigated according to the suggestions made in the past for the Phébus tests [10, 28–32]. The increase of the aerosol density has an inverse effect with respect to the increase of the dynamic shape factor: with the same dimensions, particles with a higher density have a higher weight, and heavier particles tend to deposit faster. Comparable results were found for both codes and for each test, but it was noted that employing density values below 3,000 kg/m^3 all the results present almost the same behavior.

After the analyses on the aerosol density, the influences of the agglomeration shape factor and the particle sticking probability were investigated. Both codes suggest a default value of 1 for both parameters [25, 33], but smaller and

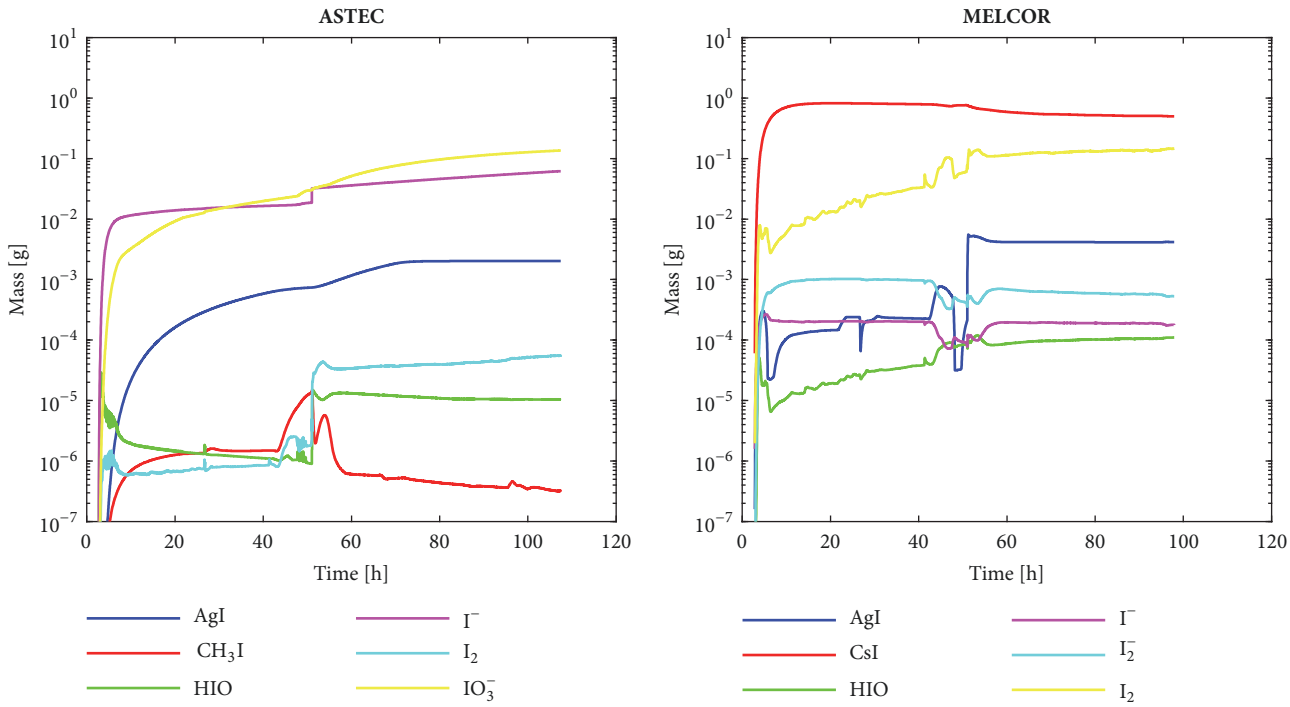

Figure 16: Iodine speciation in the sump water during the Phébus FPT-3 test.

higher values were investigated as well. The finding of this analysis was similar to that about the aerosol density: higher agglomeration factor or particle sticking probability lead to a faster depletion of the aerosol mass in the CV atmosphere.

Then, a study on the turbulence dissipation rate value was performed. Different default values are suggested for ASTEC (0.02 m^2/s^3) and MELCOR (0.001 m^2/s^3) [25, 33]. In both codes, the default value was set 0.02 m^2/s^3 and values spanning from 0.001 up to 0.02 m^2/s^3 were investigated. No appreciable differences were shown among the different cases except for the FPT-2 case where MELCOR showed somewhat better results with its own default value.

Finally, the influence of the Aerodynamic Mass Median Diameter (AMMD) and its Geometric Standard Deviation (GSD) was investigated. Default values for AMMD and GSD were set according to the data reported in the test's final reports [19–22], and sensitivity studies increasing or decreasing such values of 25% were performed. The analysis on GSD showed a negligible influence for this parameter, while those on AMMD highlighted its importance. Since for almost all the tests a too fast atmospheric depletion was predicted, the decrease of AMMD reduced also the differences between the results and the experimental data.

Additional code-specific parameters were furthermore investigated, but most of them presented only a small influence on the obtained results. The only two parameters worth of mention are the partition of I^- and HIO between the containment atmosphere and the sump: in the FPT-0 and FPT-1 tests—characterized by a nonevaporating sump at pH 5—the activation of I^- and HIO partitioning changes the iodine speciation in the sump water and the mass of iodine suspended in the containment atmosphere. However, the new speciation is still far from the expected one, and the suspended iodine mass is still different from the experimental data. A summary of the all the parameters investigated is shown in Table 6 together with the influence for each test.

8. Conclusions

In recent years, both the ASTEC and the MELCOR codes have been updated to implement and reflect the findings coming from new experimental campaigns. Thus, a continuous verification and validation activity is necessary to ensure that the improvements/modifications introduced are valuable also for the analysis of older experiments, such as the Phébus FP tests. In the past, these Phèbus tests were widely investigated in independent works [7–12] or in international benchmark exercise [34, 35]. Most of these activities focused on the degradation phenomena of the fuel bundle, and the subsequent release, and transport of FPs into the primary circuit. Among the few works analyzing the containment aspects, none of them proposed a comparison among ASTEC and MELCOR codes against the four Phébus FPT tests at once. For this reason, a comparative analysis of the two codes against these four Phébus FPT tests has been performed at the University of Pisa, and the present paper summarizes the main results achieved. Extended containment thermal-hydraulic and aerosol analyses have been then carried out, also performing a quite extended set of sensitivity analysis on the main parameters influencing the code's predictions.

The analysis was structured to investigate the four tests with the same detail. Three spatial nodalisations were created: a coarse model devoted to test the quality of the imposed boundary conditions and two refined models to investigate

Table 6: Summary of the investigated parameters and influence for each Phébus test.

Parameter	FPT-0		FPT-1		FPT-2		FPT-3	
Common parameters								
	AS	**ME**	**AS**	**ME**	**AS**	**ME**	**AS**	**ME**
Number of Particle Size Classes	*No*	*No*	**Yes**	*No*	*No*	*No*	*No*	*No*
Dynamic Shape Factor for Agglomeration Processes	**Yes**	**Yes**	**Yes**	**Yes**	**Yes**	**Yes**	**Yes**	**Yes**
Aerosol density	**Yes**	**Yes**	**Yes**	**Yes**	**Yes**	**Yes**	**Yes**	**Yes**
Agglomeration shape factor	**Yes**	**Yes**	**Yes**	**Yes**	**Yes**	**Yes**	**Yes**	**Yes**
Turbulence dissipation rates	*No*	**Yes**	*No*	*No*	*No*	**Yes**	*No*	*No*
Particle sticking probability	**Yes**	**Yes**	*No*	**Yes**	*No*	**Yes**	*No*	**Yes**
Ratio of the thermal conductivity of the gas phase to the thermal conductivity of the aerosol particles	*No*	*No*	**Yes**	*No*	*No*	*No*	*No*	*No*
Aerodynamic Mass Median Diameter	**Yes**	**Yes**	*No*	**Yes**	**Yes**	**Yes**	**Yes**	**Yes**
Geometric Standard Deviation	*No*	*No*	**Yes**	*No*	*No*	*No*	*No*	*No*
ASTEC-specific parameters								
Influence of the aerosol particles on the gas density	*No*	/	*No*	/	*No*	/	*No*	/
Flag to dynamically calculate the condensation time step	*No*	/	*No*	/	*No*	/	*No*	/
Air molecular weight	*No*	/	*No*	/	*No*	/	*No*	/
Relation employed to calculate the collision efficiency for gravitational and turbulent coagulation	**Yes**	/	*No*	/	*No*	/	*No*	/
Water film thickness used for drainage and aerosol wash-down	*No*	/	*No*	/	*No*	/	*No*	/
Aerosol deposition velocity for each aerosol component	*No*	/	*No*	/	*No*	/	*No*	/
MELCOR-specific parameters								
Condensation of water on all the aerosol particles or only on aerosol particles containing water	/	*No*	/	*No*	/	*No*	/	*No*
Particle slip coefficient influencing the gravitational deposition	/	*No*	/	*No*	/	*No*	/	*No*
Constant associated with the thermal accommodation coefficient for the thermophoresis deposition mechanism	/	*No*	/	*No*	/	*No*	/	*No*
Diffusion boundary layer thickness	/	*No*	/	*No*	/	*No*	/	*No*
Partition of I- between atmosphere and sump	/	**Yes**	/	**Yes**	/	/	/	*No*
Partition of HIO between atmosphere and sump	/	**Yes**	/	**Yes**	/	*No*	/	*No*

the influence of the CV vertical and radial subdivision. Slight differences exist between the ASTEC and MELCOR nodalisations to exploit the different modelling approaches characterizing the two codes: for instance, in ASTEC, the condensate falls down on the bottom of the volume and then drained away with specific junctions, while in MELCOR the condensate is drained from the bottom of each wall to the sump water through other walls.

Only the results of the most complex nodalisation were shown in the paper being the closest to the experimental data. In general, a good agreement is shown between the code's thermal-hydraulics predictions and experimental data. Though, a strong influence of nodalisation choices and user's assumption was highlighted as already suggested in precedent works [7, 28, 36]. A clear example of this influence is shown at the end of the aerosol phase in each test: during this time interval, the sump water and the superficial wet condenser's temperatures are modified to prepare the CV for the incoming washing phase. These two actions influence the total pressure which presents an initial decrease due to the enhanced condensation followed by a pressure increase due to the noncondensable gas ingress. In both codes, this trend is not well captured because of the too strong influence of the condenser and sump water temperatures on the CV atmosphere, and the origin of this difference probably lies in the employed nodalisations/user's choices being almost identical in both codes and in all the four tests. A sensitivity study on the wall's characteristic length in MELCOR was also performed to fill the gaps occurring between the code's predictions and the experimental data in the FPT-0 and FPT-2 tests. This analysis suggested that this parameter is strongly correlated with the employed spatial nodalisation and with the investigated transient; thus the definition of a "good" value capable of well reproducing each test was not possible.

The FP and SM evolution in the CV are another aspect of main importance in the Phébus tests. The FP and SM mass evolution depends on local thermal-hydraulics conditions, different agglomeration processes, and eventual resuspension

processes. The combination of all these phenomena is the main difference between the Phébus FPT tests and other simpler tests. The results obtained with both codes show a slightly too fast FP and SM deposition for all the investigated tests, but the predictions can be still considered quite acceptable. The sensitivity analysis performed also suggested that most of the investigated input parameters have only a minor influence on the overall results. The few parameters affecting the results were the aerosol density, the agglomeration shape factor, the particle sticking probability, the turbulence dissipation rate, and the AMMD. For all of them, the utilization of the code default value (if available) can be suggested since they provided the best agreement with the experimental data.

The iodine mass evolution in the CV atmosphere was also investigated. A cycle of volatile iodine compounds destruction and creation is established in each test due to the dose rates affecting the CV atmosphere and walls. In the FPT-2 tests, these dose rates were not defined in the input decks due to the lack of this data in the final test report [21]. The effect of this absence is well shown, since both codes fail to reproduce the creation and destruction cycle of volatile iodine compounds, thus leading to poor and unrealistic results.

Finally, the speciation of iodine in the sump water was also evaluated. Iodine speciation differs in each Phébus test according to sump pH conditions, water temperature, dose rates, and available chemical species in the water. In this regard, the two codes present completely different results mainly because the ASTEC implements the most recent findings on iodine chemistry [26], while MELCOR still presents modelling approaches anchored to older researches [27].

As general conclusion, it can be stated the ASTEC presents better results than MELCOR, especially regarding the iodine behavior both in the atmosphere and in the sump water. Further developments seem still necessary for specific thermal-hydraulic phenomena (drop-wise condensation) as well as for models affecting the FP and SM behavior, but—compared to the results shown in most of the precedent works—the overall results of the present works seem slightly closer to the experimental ones even if some user's effects are still present. This probably means that the improvements introduced in both codes in the latest versions reduce the influence of these user's effects and reduce the differences between the calculated and experimental results. Then, it can be stated that the improvements implemented in the latest code versions, deriving from more recent experimental campaigns, positively affect also the reproduction of older tests such as the Phébus FP tests.

Data Availability

The experimental data used in the present paper have been already published in several papers.

Disclosure

Bruno Gonfiotti is now at Karlsruhe Institut für Technologie, Institut für Neutronenphysik und Reaktortechnik (INR), Hermann-von-Helmholtz-Platz 1, 76344, Eggenstein-Leopoldshafen, Germany. Mail is bruno.gonfiotti@kit.edu.

Conflicts of Interest

The authors declare that they have no conflicts of interest.

References

[1] B.R. Sehgal, "Light water reactor safety. A historical review," in *Nuclear Safety in Light Water Reactors*, Elsevier, 2012.

[2] B. Clément and R. Zeyen, "The objectives of the Phébus FP experimental programme and main findings," *Annals of Nuclear Energy*, vol. 61, pp. 4–10, 2013.

[3] P. March and B. Simondi-Teisseire, "Overview of the facility and experiments performed in Phébus FP," *Annals of Nuclear Energy*, vol. 61, pp. 11–22, 2013.

[4] O. De Luze, T. Haste, M. Barrachin, and G. Repetto, "Early phase fuel degradation in Phébus FP: Initiating phenomena of degradation in fuel bundle tests," *Annals of Nuclear Energy*, vol. 61, pp. 23–35, 2013.

[5] T. Haste, F. Payot, and P. D. W. Bottomley, "Transport and deposition in the Phébus FP circuit," *Annals of Nuclear Energy*, vol. 61, pp. 102–121, 2013.

[6] M. Laurie, P. March, B. Simondi-Teisseire, and F. Payot, "Containment behaviour in Phébus FP," *Annals of Nuclear Energy*, vol. 60, pp. 15–27, 2013.

[7] G. Gyenes and L. Ammirabile, "Containment analysis on the PHEBUS FPT-0, FPT-1 and FPT-2 experiments," *Nuclear Engineering and Design*, vol. 241, no. 3, pp. 854–864, 2011.

[8] F. Martín-Fuertes, R. Barbero, J. M. Martín-Valdepeñas, and M. A. Jiménez, "Analysis of source term aspects in the experiment Phebus FPT1 with the MELCOR and CFX codes," *Nuclear Engineering and Design*, vol. 237, no. 5, pp. 509–523, 2007.

[9] H.-C. Kim, S.-B. Kim, J.-H. Park, and S.-W. Cho, "Analysis of Phébus FP experiments in Korea," *Annals of Nuclear Energy*, vol. 61, pp. 215–224, 2013.

[10] L. E. Herranz, M. Vela-García, J. Fontanet, and C. L. D. Prá, "Experimental interpretation and code validation based on the PHEBUS-FP programme: Lessons learnt from the analysis of the containment scenario of FPT1 and FPT2 tests," *Nuclear Engineering and Design*, vol. 237, no. 23, pp. 2210–2218, 2007.

[11] A. Kontautas and E. Urbonavičius, "Analysis of aerosol deposition in PHEBUS containment during FPT-1 experiment," *Nuclear Engineering and Design*, vol. 239, no. 7, pp. 1267–1274, 2009.

[12] J.-H. Park, D.-H. Kim, and H.-D. Kim, "Summary of the Results From the Phebus Fpt-1 Test for a Severe Accident and the Lessons Learned With Melcor," *Nuclear Engineering and Technology*, vol. 38, pp. 535–550, 2006.

[13] G. Weber, L. E. Herranz, M. Bendiab et al., "Thermal-hydraulic-iodine chemistry coupling: Insights gained from the SARNET benchmark on the THAI experiments Iod-11 and Iod-12," *Nuclear Engineering and Design*, vol. 265, pp. 95–107, 2013.

[14] J.-P. Van Dorsselaere, A. Auvinen, D. Beraha et al., "Recent severe accident research synthesis of the major outcomes from the SARNET network," *Nuclear Engineering and Design*, vol. 291, pp. 19–34, 2015.

[15] B. Gonfiotti and S. Paci, "Stand-Alone containment analysis of the phébus FPT tests with the ASTEC and the MELCOR codes:

The FPT-0 Test," *Science and Technology of Nuclear Installations*, vol. 2017, 2017.

[16] B. Gonfiotti and S. Paci, "Stand-alone containment analysis of the Phébus FPT-1 test with the ASTEC and the MELCOR codes," *Journal of Nuclear Engineering and Radiation Science*, vol. 4, no. 2, 2018.

[17] B. Gonfiotti and S. Paci, "Stand-alone containment analysis of Phébus FPT tests with ASTEC and MELCOR codes: the FPT-2 test," *Heliyon*, vol. 4, no. 3, 2018.

[18] B. Gonfiotti and S. Paci, "Stand-alone Containment Analysis of the Phébus FPT-3 test with the ASTEC and the MELCOR codes," in *Proceedings of the 26th Int. Conf. Nucl. Eng.*, London (UK), 2018.

[19] N. Hanniet-Girault and G. Repetto, "FPT-0 final report," *Saint-Paul-lez-Durance (F)*, 1999.

[20] D. Jacquemain, S. Bourdon, A. de Braemaeker, and M. Barrachin, "Final report FPT-1," *Saint-Paul-lez-Durance (F)*, 2000.

[21] A.-C. Gregoire, P. March, F. Payot et al., "PHEBUS FP FPT2 Final Report," Saint-Paul-lez-Durance (F), 2008.

[22] F. Payot, T. Haste, B. Biard et al., "PHEBUS FP FPT3 Final Report," Saint-Paul-lez-Durance (F), 2011.

[23] W. Klein-Hessling and B. Schwinges, *ASTEC V0 CPA Module Program Reference Manual, Institut de Protection et de Surete Nucleaire (IRSN - France) / Gesellschaft fur Anlagen-und Reacktorsicherheit mbH*, Germany, 1998.

[24] J. Phillips, A. Notafrancesco, and J. L. Tills, *Application of the MELCOR Code to Design Basis PWR Large Dry Containment Analysis*, 2009.

[25] L. L. Humphries, V. G. Figueroa, M. F. Young, D. Louie, and J. T. Reynolds, "MELCOR Computer Code Manuals Vol. 1: Primer and User's Guide," SAND2015-6691 R, Albuquerque, USA, 2015.

[26] B. Clément, L. Cantrel, G. Ducros et al., *State of the Art report on Iodine Chemistry*, 2007.

[27] L. Soffer, S. Burson, C. Ferrell, R. Lee, and J. Ridgely, *Accident Source Terms for Light-Water Nuclear Power Plants*, Washington, WA, USA, 1995.

[28] A. Kontautas and E. Urbonavičius, "Uncertainty and sensitivity evaluation of aerosol deposition in PHEBUS containment during FPT-2 experiment," *Energetika*, vol. 61, no. 1, 2015.

[29] A. Kontautas, E. Babilas, and E. Urbonavičius, "COCOSYS analysis for deposition of aerosols and fission products in PHEBUS FPT-2 containment," *Nuclear Engineering and Design*, vol. 247, pp. 160–167, 2012.

[30] I. Kljenak and B. Mavko, "Simulation of Containment Phenomena during the Phebus FPT2 Test with the CONTAIN Code in," in *Proceedings of the Proc. Int. Conf. Nucl*, p. 417, 2009.

[31] E. Hontanon, J. Polo, and L. E. Herranz, "On the modelling capabilities to simulate aerosol behaviour in the PHEBUS-FP containment: Lessons learned from FPT0 test," *Journal of Aerosol Science*, vol. 27, no. 1, pp. S459–S460, 1996.

[32] P. Dumaz and S. Cho, "Thermophoretic deposition in the first Phebus-FP experiment," *Journal of Aerosol Science*, vol. 26, pp. 83-84, 1996.

[33] G. Weber, *ASTEC V0 Description of Aerosol Models in the Containment Part of ASTEC (CPA)*, 1999.

[34] K. Mueller, S. Dickinson, C. de Pascale et al., "Validation of severe accident codes on the phebus fission product tests in the framework of the PHEBEN-2 project," *Nuclear Technology*, vol. 163, no. 2, pp. 209–227, 2008.

[35] M. Di Giuli, T. Haste, R. Biehler et al., "SARNET benchmark on Phébus FPT3 integral experiment on core degradation and fission product behaviour," *Annals of Nuclear Energy*, vol. 93, pp. 65–82, 2016.

[36] F. De Rosa and R. Mari, "Thermal-hydraulics and physics near Phebus condenser, a comparison between codes and against some epxerimental data from FPT0 test," in *Proceedings of the 7th Int. Conf. Nucl. Eng. (7th ICONE)*, Tokyo, 1999.